

# Quantum parameter estimation with uncertainty quantification from continuous measurement data using neural network ensembles

Amanuel Anteneh\*

Department of Physics, University of Virginia, 382 McCormick Rd, Charlottesville, VA 22903, USA

(Dated: March 9, 2026)

We show that ensembles of deep neural networks, called deep ensembles, can be used to perform quantum parameter estimation while also providing a means for quantifying uncertainty in parameter estimates, which is a key advantage of using Bayesian inference for parameter estimation that is lost when using existing machine learning methods. We show that optimizing for both accurate parameter estimates and well calibrated uncertainty estimates does not lead to degradation in the former as opposed to only optimizing for accuracy. We also show that the drift detection capabilities of these ensemble models can be used to detect drift in the experimental data used during inference. This approach is also shown to provide much faster inference time than both likelihood-based and likelihood-free Bayesian inference. These results suggest that such models could enable accurate, real-time parameter estimation with quantified uncertainty, making them promising candidates for deployment in experimental settings.

## I. INTRODUCTION

The precise estimation of physical parameters is of central importance in quantum information science and physics more broadly [1, 2]. It is particularly relevant to the field of quantum metrology which itself has been instrumental for making discoveries in fundamental physics. For example, squeezed-state based metrological methods have been used for gravitational wave detection [3–5] and dark matter axion searches [6–8]. Quantum parameter estimation procedures generally have three steps: i) a quantum probe system is prepared in some initial state  $\rho_0$ ; ii) the unknown parameter(s)  $\theta$  are encoded into the state of the probe system using some unitary transformation  $U(\theta)\rho_0U^\dagger(\theta)$ ; iii) a measurement is performed on the probe system and the measurement result is used to extract information about the unknown parameter(s). This process is then repeated multiple times to gather more measurement data to improve the precision of the estimation [1].

A popular approach for performing quantum parameter estimation is based on Bayesian inference [9–11]. This approach provides benefits such as uncertainty quantification for parameter estimates, a natural mechanism by which one can incorporate prior knowledge about the parameter into the analysis, and, perhaps most importantly, the ability to provide an optimal estimator of the parameters under consideration in the limit of a large enough number of measurements [10, 11]. However, this approach also comes with significant drawbacks.

Firstly, Bayesian inference protocols generally require derivation of an analytic expression of the likelihood distribution that the measurement data is assumed to be generated from. This is not always feasible for many systems under ideal conditions and for simple systems this can become intractable when one attempts to model

the effects of experimentally imperfections. This may be circumvented by use of so-called ‘likelihood-free’ methods such as approximate Bayesian computation (ABC) [12, 13] but this method presents its own challenges such as a drastic increase in sample complexity when the number of parameters being estimated increases, requiring access to a simulator which can generate samples from the likelihood distribution, and selection of a suitable discrepancy measure (and summary statistic) for the rejection sampling routine [12, 14, 15].

Secondly, Bayesian inference time can scale poorly as the dimensionality of the problem, i.e. number of parameters being estimated, increases. This is due to the random walk behavior used by common Markov chain Monte Carlo (MCMC) methods, such as Gibbs sampling, to explore the posterior distribution. This can lead to long convergence times when the the posterior distribution is high dimensional [15]. While more sophisticated Bayesian inference methods based on the Hamiltonian Monte Carlo algorithm are more robust to this they also introduce the additional overhead of requiring gradient computations to more effectively explore the posterior distribution [15, 16]. Bayesian inference time can also scale poorly when the number of measurement results used is large [17]. For these reasons real time estimation is made difficult.

Recently approaches based on the use of machine learning (ML) algorithms, in particular neural networks (NNs), have gained popularity for performing quantum parameter estimation [18–23]. In contrast to Bayesian inference, NN based approaches provide faster inference time, owing to their highly parallelizable inference process, while retaining the benefits of likelihood-free methods like ABC as they can learn complex functions from input-output pairs of training examples due to their high expressive power [24]. Furthermore, the ABC-based estimation method presented in Ref. [13] requires the *a priori* preparation of multiple sets of measurement results for different values of  $\theta$  to perform inference. While an ML approach also requires this for the initial model

---

\* asa2rc@virginia.edu

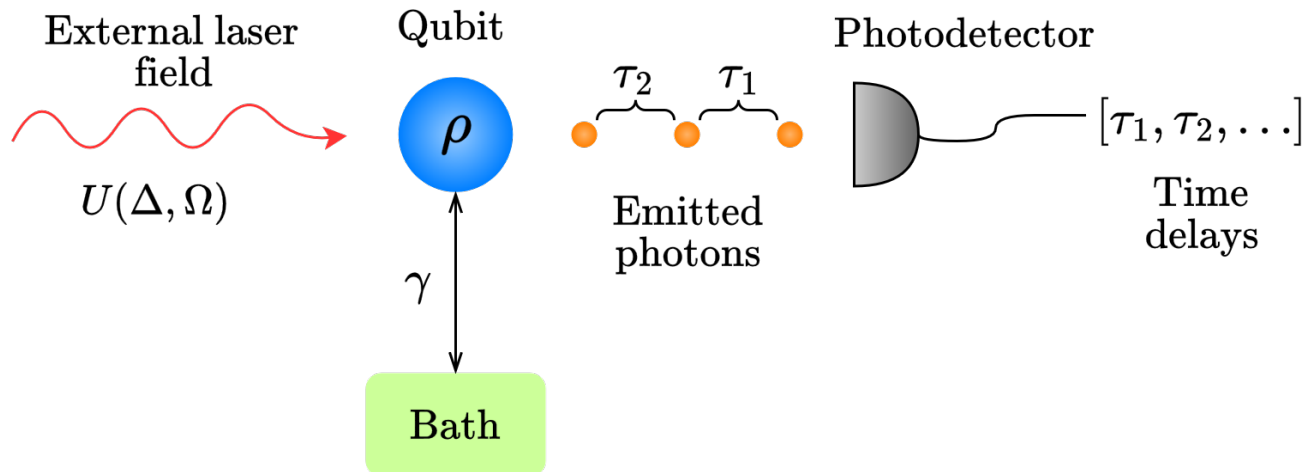


FIG. 1: Diagram of quantum parameter estimation procedure using continuous photon counting measurement of a two-level system (qubit) coupled to an external bath (the environment) with coupling strength  $\gamma$  and continuously driven by an external laser field.

training phase it is typically no longer needed at inference time unlike the ABC method. In Ref. [21] it was shown that a NN can be trained to perform parameter estimation given input-output pairs of quantum measurement results from a continuous measurement of a quantum probe system and the corresponding parameter values which generated those measurement results. This approach however utilized a large amount of training data and only provides point estimates without uncertainty quantification. Here we extend this approach to provide uncertainty estimates, thereby retaining a benefit of Bayesian approaches, and also drastically reducing the amount of training data required to train the model. We also study the robustness of our method to different types of noise in the training data and measurement results provided to the model at inference time.

## II. QUANTUM SYSTEM

As a specific example we study the system from Refs. [9, 10, 13, 21], shown in Fig. 1, which consists of a two-level system (TLS) with states  $\{|g\rangle, |e\rangle\}$  and transition frequency  $\omega_q$  which is continuously driven by an external laser field with frequency  $\omega_L$ . The TLS is also coupled to the environment which results in dissipative interactions that give rise to stochastic photon emission with rate  $\gamma$ . The dynamics of this system can be described by the Lindblad master equation [9] (where  $\hbar = 1$ )

$$\frac{\partial}{\partial t} \hat{\rho}(t) = -i[\hat{H}, \hat{\rho}(t)] + \gamma \hat{L} \hat{\rho}(t) \hat{L}^\dagger - \frac{\gamma}{2} \{ \hat{L}^\dagger \hat{L}, \hat{\rho}(t) \} \quad (1)$$

where, in the reference frame rotating at the frequency of the laser, the Hamiltonian  $\hat{H}$  can be written as

$$\hat{H} = \Delta \hat{\sigma}^\dagger \hat{\sigma} + \Omega (\hat{\sigma} + \hat{\sigma}^\dagger). \quad (2)$$

Here  $\Delta \equiv \omega_q - \omega_L$  and  $\Omega$  are the laser-atom detuning and the Rabi frequency respectively,  $\gamma$  is the rate at which the excited state of the TLS decays to the ground state  $|g\rangle$ , thus emitting a photon,  $\hat{\sigma} = |g\rangle \langle e|$  is the TLS lowering operator and the Lindblad jump operator is set as  $\hat{L} = \hat{\sigma}$ .

The first term in Eq. 1 corresponds to the unitary dynamics of the system governed by the Hamiltonian  $\hat{H}$  while the last two terms model the dissipative dynamics of the TLS's interaction with the environment. The second term corresponds to the collapse of the TLS to the ground state which coincides with the measurement of a spontaneously emitted photon. The anti-commutator term corresponds to the dissipative dynamics in the absence of photon detection [9]. It was first shown in Ref. [9] that measurements of the time delays between consecutive photon detections on the system could be used to estimate the parameters  $\Delta$  and  $\Omega$  using Bayesian inference.

## III. MACHINE LEARNING EXPERIMENTS

We train and test our models for predicting the detuning parameter  $\Delta$  with the same dataset used in [21]. As such the inputs to our NNs are a set of time delays  $x = [\tau_1, \dots, \tau_N]$  where  $N = 48$  which were generated using the Monte Carlo method of quantum trajectories with the QuTiP library [25]. The decay rate is assumed to be known at  $\gamma = 1$  and that  $\Omega = \gamma$ . All models were implemented using the PyTorch library and we utilized the automatic mixed precision training method provided by PyTorch to reduce memory overhead [26, 27]. All training ran on an NVIDIA GeForce RTX 2070 Super GPU.

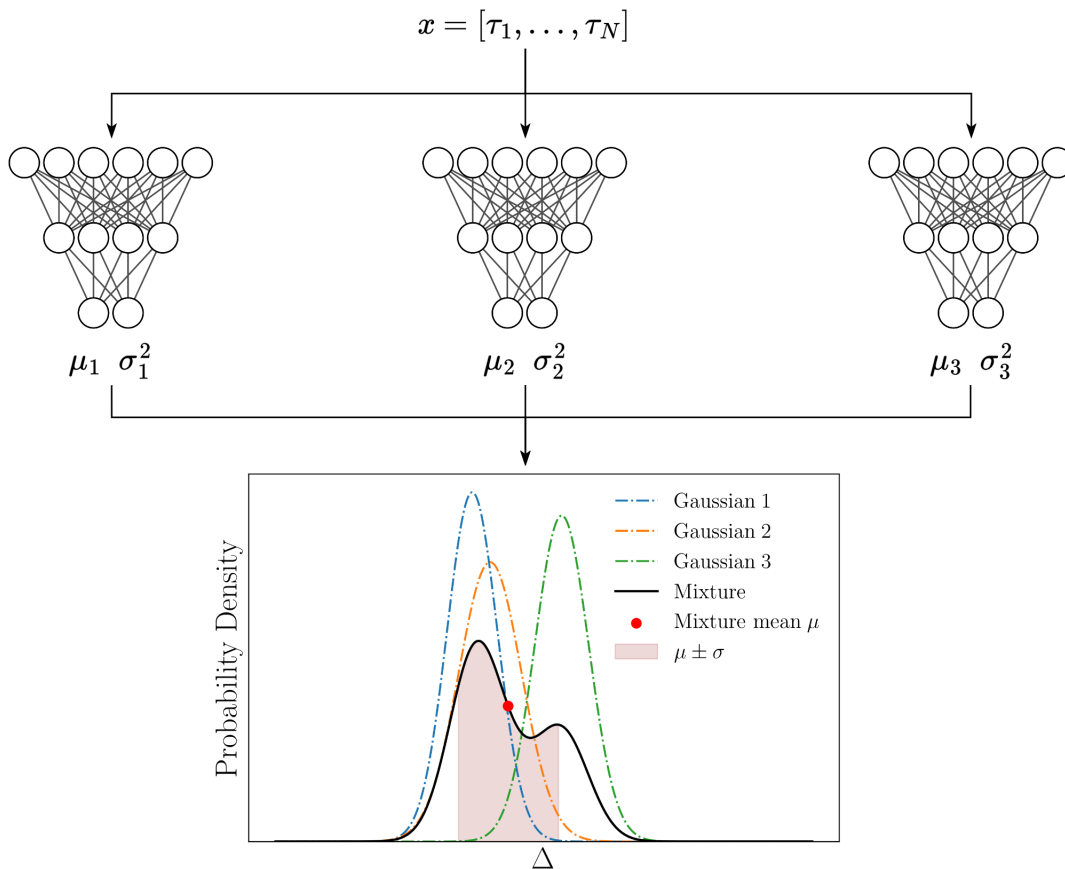


FIG. 2: Diagram of using deep ensemble of  $M = 3$  NNs for estimating the detuning parameter  $\Delta$  from a set of input time delay measurements  $x = [\tau_1, \dots, \tau_N]$  from a quantum trajectory.

### A. Deep ensembles

Model ensembling is a simple but powerful method in machine learning. Ensemble methods employ multiple models, typically ‘weak learners’ as individually these models have suboptimal performance, to create a single overall model by aggregating the predictions of the component models. The resulting model often has better performance, in terms of both bias and variance, than the individual models in isolation [28]. A state-of-the-art method for predictive uncertainty quantification for deep learning based models are deep ensembles [17, 29, 30]. These models quantify epistemic (model) uncertainty, i.e. uncertainty that arises from the choice of model parameters, due to the use of an ensemble of independent models. This type of uncertainty is reducible if one can procure more data. They also quantify aleatoric (data) uncertainty, i.e. uncertainty that is inherent to the process which produces the training data, by being trained to minimize a negative log likelihood loss function [17, 31, 32]. Unlike model uncertainty, data uncertainty is not reducible [31]. For regression problems, such as the one considered in this work, deep ensembles work by training  $M$  independent NNs to learn a continu-

ous probability distribution over predictions. The overall model is then treated as a mixture of these distributions. Model diversity emerges from the random initialization of each network at the start of training as well as the randomness from the mini-batch sampling that occurs during training via stochastic gradient descent.

Deep ensembles are preferable to Bayesian NNs (BNNs) [14], which are another common tool for quantifying uncertainty in deep learning, for two reasons. Firstly they require minimal changes to the standard NN training process and their training is easily scalable via parallelization since each network in the ensemble can be trained completely independently. Secondly BNNs face the same computational problem as Bayesian inference in general i.e. the intractability of computing the posterior distribution over model parameters exactly [14, 29]. In fact due to the large number of parameters in NNs standard Bayesian sampling methods like MCMC are often too computationally expensive to use for BNN training and methods such as variational inference, which are faster but have weaker theoretical guarantees compared to MCMC, must be used [17].

## B. Model training

We benchmark our deep ensembles against Bayesian inference as well as single NNs. All NNs use the same architecture, with the exception of the input layer, as the *Hist-Dense* network in Ref. [21] with three hidden layers of size 100, 50, and 30 respectively using ReLU activation functions. For the input layer of all our models we use a custom layer that implements a smoothed histogram based on ideas from kernel density estimation [28]. This introduces an inductive bias into the model i.e. that the ordering of the input time delays has no significance as the TLS is reset to the ground state in the event of a photon detection so the time delay measurements are independent and identically distributed [33]. This also allows the NN to process inputs of arbitrary length which is useful for when varying numbers of time delay measurements are made [21]. We use equally spaced bins where the density at bin  $b$  is given by a sum over all values in the sample in the form of the Gaussian kernel

$$f(b) = \sum_{i=0}^N \exp\left(-\frac{(\tau_i - b)^2}{2\phi^2}\right) \quad (3)$$

where  $\phi^2$ , sometimes called the bandwidth, is a learnable parameter which controls the smoothness of the resulting estimated kernel density and we use the same range for the histogram,  $\tau_{\min} = 0$  and  $\tau_{\max} = 100/\gamma$ , as in [21]. We treat the number of bins as a tunable hyperparameter.

Using the deep ensemble we seek to learn a distribution  $P(\Delta|\tau_1, \dots, \tau_N)$  over values of  $\Delta$  given the time delay measurements from a quantum trajectory as shown schematically in Fig. 2. We approximate this distribution as an evenly weighted mixture of  $M = 10$  Gaussian distributions and have the  $m$ -th NN in the ensemble learn the mean,  $\mu_m$ , and variance,  $\sigma_m^2$ , of the  $m$ -th component distribution by minimizing the Gaussian negative log likelihood loss [29]

$$\mathcal{L}(y, \mu, \sigma^2) = \frac{1}{2} \log(\sigma^2) + \frac{(y - \mu)^2}{2\sigma^2} + \text{constant} \quad (4)$$

where  $y = \Delta$  is the ground truth detuning parameter value for the trajectory-parameter pair  $([\tau_1, \dots, \tau_N], \Delta)$ . The prediction for the parameter is then taken to be the mean of the mixture while the predictive uncertainty is quantified by the variance of the mixture. These quantities are given by

$$\mu(x) = \frac{1}{M} \sum_m \mu_m(x) \quad (5)$$

$$\sigma^2(x) = \frac{1}{M} \sum_m (\sigma_m^2(x) + \mu_m^2(x)) - \mu(x) \quad (6)$$

respectively [29]. A useful property of Gaussian mixtures is that they are universal approximators for probability densities [34]. Note, however, that the log likelihood need

not be that of a Gaussian, the negative log likelihood of any probability distribution may be used if deemed appropriate and one is able to compute the relevant moments.

An alternative approach to training an ensemble of  $M$  NNs would be to simply train each network to minimize the mean squared error (MSE) loss function. The uncertainty estimates would then be computed as the empirical variance of the predictions made by the  $M$  networks. While this approach is more straightforward it leads to the model producing highly overconfident uncertainty estimates as MSE only optimizes for predictive accuracy and not predictive uncertainty [29]. This highlights the crucial role played by selection of a proper loss function like the Gaussian negative log likelihood in training a deep ensemble to produce properly calibrated uncertainty estimates.

## C. Hyperparameter Tuning

Ref. [21] trained single NNs on a dataset of  $4 \times 10^6$  trajectory-parameter pairs [35]. With the use of hyperparameter tuning we are able to achieve the same level of performance with only 1% ( $4 \times 10^4$ ) of the original training data. This is also much lower than the amount of data needed for ABC which used 1000 trajectories generated for 100 different values of  $\Delta$  which results in a total dataset size of  $10^5$  [13, 36]. Note also that the ABC approach used longer trajectories with  $N = 200$  time delay measurements as opposed to the  $N = 48$  used in this work. We split the training data into training and validation sets with a 80% and 20% split respectively. A commonly used approach to train ensemble models is the use of bootstrap aggregation (bagging) which consists of training ensemble members on different bootstrapped samples of the original dataset. However, this is mainly advantageous for ensemble models comprised of weak learners, such as tree-based ensemble models, and worsens performance when used to training ensembles of strong learners like deep neural networks [29, 37]. We therefore did not utilize bagging in our experiments.

We use the tree-structured Parzen estimator optimization algorithm provided by the `Optuna` framework to perform hyperparameter tuning of the single network models presented in this work [38]. We utilize both trail pruning and early stopping during our tuning and training processes respectively and tune for 20 trials. For the single models the loss function used during training was also tuned as part of the hyperparameter tuning process with the possible choices being the root mean squared error (RMSE) loss or the mean squared logarithmic error (MSLE) loss [21]. Further details on the tuned hyperparameters can be found in Appendix B. For experiment tracking, validation metric logging, and model storage we utilize the open source framework `MLflow` [39]. We make the `MLflow` logs which contain learning curve plots, model weights, and hyperparameter settings for all the

models trained in the present work available at [40].

#### D. Predictive accuracy preservation under ensembling

In this section we examine the performance of our ensemble approach based on predictive accuracy. This is crucial as we must ensure that the training of the ensemble does not sacrifice predictive accuracy in favor of well calibrated uncertainty estimates.

##### 1. Noiseless training data

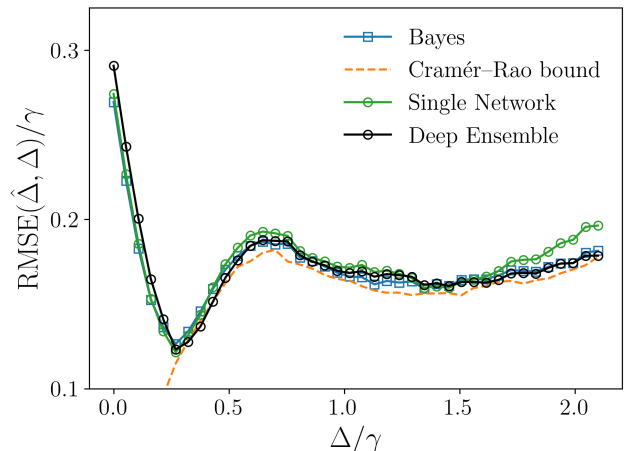
We first benchmark the deep ensemble against Bayesian inference and single NNs in the case of noiseless training data. Fig. 3a shows the Cramér–Rao bound and the error of the three estimators on the same test set of  $40 \times 10^4$  trajectories generated for 40 values of  $\Delta$ , which were uniformly chosen over the interval  $[0, 2.1\gamma]$ , used in [21]. Details on the Bayesian estimation procedure can be found in Appendix A as well as Appendix B of [21]. Since all estimators used in this work are biased we use the *biased* Cramér–Rao bound computed in Ref. [21] which is given by

$$\text{var}(\hat{\theta}) \geq \left(1 + \frac{d}{d\theta} \text{bias}(\hat{\theta})\right)^2 \frac{1}{NF(\theta)} \quad (7)$$

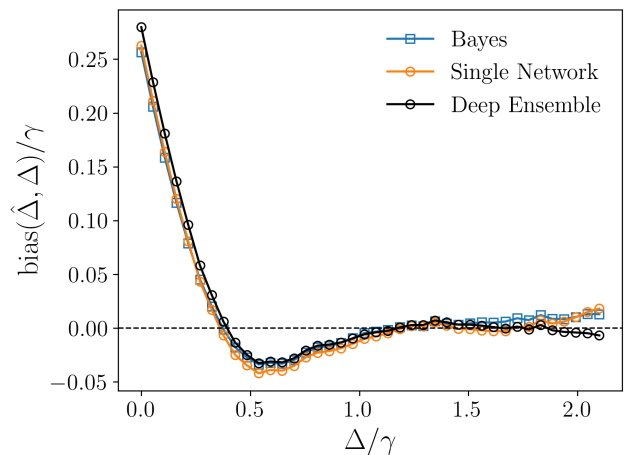
where  $F(\theta)$  is the Fisher information and  $N$  is the number of measured time delays in the sample. The bias of each estimator, defined as  $\text{bias}(\hat{\Delta}, \Delta) \equiv \mathbb{E}(\hat{\Delta}) - \Delta$  [41], can be seen in Fig. 3b. We can see that the deep ensemble model outperforms or is competitive with the single network model and that the deep ensemble saturates the Cramér–Rao bound for more values of  $\Delta$  than compared to the single model. This is particularly notable because, unlike the single model’s loss function, the ensemble model’s loss function optimizes not only for predictive error but also for predictive uncertainty.

##### 2. Noise in time delay measurements

For real data from an experimental setup there is likely to be noise from various sources. One such source of noise would be time jitter [21, 42]. It was shown in Ref [21] that, as expected, Bayesian inference that does not account for this noise in its likelihood model performs very poorly and is outperformed by a NN that is trained on data with this noise. We evaluate the robustness of our estimator to this noise by modifying the input time delays used for training and testing of our models as  $x \rightarrow x + x_{\text{noise}}$  where  $x_{\text{noise}}$  is a Gaussian noise term  $x_{\text{noise}} \sim \mathcal{N}(0, \sigma_\tau)$ . Fig. 4 shows the results for training data with time jitter noise following the Gaussian distribution  $\mathcal{N}(0, \sigma_\tau = 0.76)$  with the Bayesian inference



(a) Average RMSE of various estimation strategies plotted with the biased Cramér–Rao bound.



(b) Bias of various estimation strategies.

FIG. 3: Performance of different estimators on  $\Delta$  estimation task.

results for noiseless and noisy input data shown for reference. As expected the Bayesian estimator that does not take into account the time jitter noise performs significantly worse than the noiseless Bayesian estimator. We can see that the deep ensemble is again competitive with or outperforms the single model for all values of  $\Delta$ .

##### 3. Noise in ground truth parameter values

Another question addressed in Ref. [21] was whether an NN can learn to perform parameter estimation robustly in the presence of noise in the training labels. This could, for example, occur if the method used to generate the training labels, i.e. the measurement device, had less than ideal precision. This noise was modeled by adding a Gaussian noise term  $\mathcal{N}(0, \sigma_y)$  to the training labels. Ro-

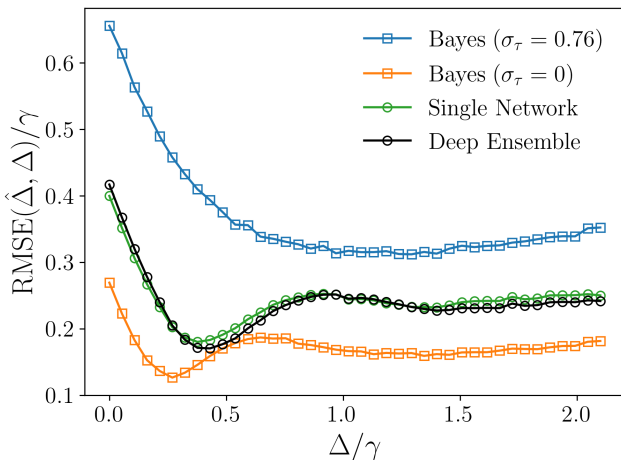
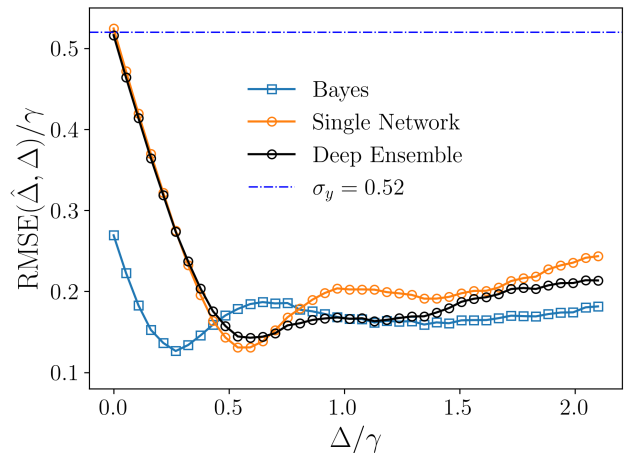


FIG. 4: Performance of single network and deep ensemble in the presence of time jitter noise in the training and testing data following a Gaussian distribution  $\mathcal{N}(0, \sigma_\tau = 0.76)$ .

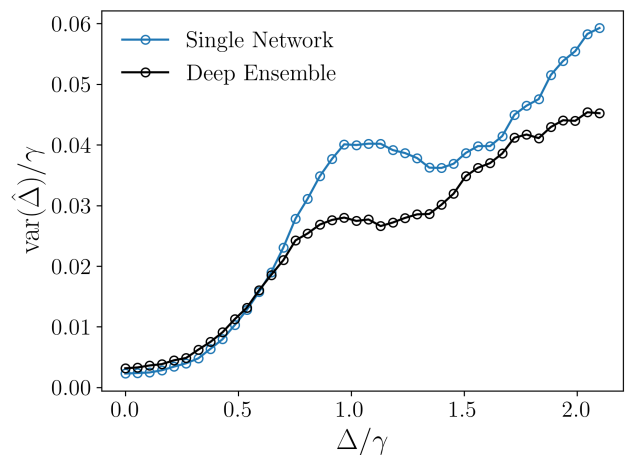
bustness is defined as being able to make predictions with an RMSE lower than that of the standard deviation  $\sigma_y$  of the Gaussian noise in the training labels of  $\Delta$ . It was found that a single NN is indeed robust to such noise [21]. A natural question would then be whether this robustness is retained when using a deep ensemble. Fig. 5a answers this question in the affirmative. In fact the deep ensembles achieves better performance than the single model for most values of  $\Delta$ . This increased robustness to perturbations in the training labels is expected as it is a well known strength of ensemble models that they generally have lower variance than the individual ensemble members [43]. This is explicitly shown in Fig. 5b, where the variance of an estimator is given by  $\text{var}(\hat{\theta}) \equiv \mathbb{E}[\hat{\theta}^2] - \mathbb{E}[\hat{\theta}]^2$  [41], which shows that the deep ensemble generally has lower variance than the single network.

### E. Data shift

For ML models which are discriminative models such as the ones used here we assume the input-output pairs, i.e. the data,  $(X, Y)$  are generated from some joint distribution  $P(X, Y)$  which can be factored into  $P(X)P(Y|X)$  [14]. An important consideration is how models which are trained on training data generated from one distribution  $P(X, Y)$  perform on data generated from a different distribution  $Q(X, Y)$  such that  $P(X, Y) \neq Q(X, Y)$ . This phenomena is often seen in ML models deployed in real world settings and is called data shift or data drift, with the data coming from the new distribution being called out-of-distribution samples, and often results in the model performance degrading [44].



(a) Performance of single network and deep ensemble in the presence of noise in the training data labels following a Gaussian distribution  $\mathcal{N}(0, \sigma_y = 0.52)$ .



(b) Variance of single network model and deep ensemble trained on data with noisy labels.

FIG. 5: Performance of different estimators on  $\Delta$  estimation task with noise present in training labels.

#### 1. Robustness to covariate shift

One such example of this kind of data shift is covariate shift [14, 44, 45]. In this case the marginal distribution of the input features  $P(X) = P(\tau_1, \dots, \tau_N)$  changes while the conditional distribution of outputs given these input features  $P(Y|X) = P(\Delta|\tau_1, \dots, \tau_N)$  remains unchanged. For the current estimation task one such example would be the time jitter noise examined previously. In the case of time jitter one can view the perturbed time delay measurements as what are called adversarial examples [46]. Adversarial examples are inputs to the model which have been slightly perturbed in such a way that they cause the model to produce incorrect predictions [34]. To improve robustness to adversarial examples deep ensembles

can incorporate an adversarial component to the training process via use of the fast gradient sign method [29, 33]. This consists of generating an adversarial example  $x'$  for a given input  $x$  as

$$x' = x + \epsilon \text{sign}(\nabla_x(\mathcal{L}(y, x))) \quad (8)$$

where  $\epsilon$  is typically taken to be 1% of the input range of corresponding input feature. The loss function used during training is then  $\mathcal{L}(y, \hat{y}) + \mathcal{L}(y, \hat{y}')$  where  $\hat{y}$  and  $\hat{y}'$  are the model predictions for  $x$  and  $x'$  respectively and  $y$  is the ground truth label.

To evaluate the robustness of the NNs to this kind of data shift we train a single network model and an adversarial deep ensemble on data *without* time jitter noise and test the models on covariate shifted data which includes time jitter noise with  $\sigma_\tau = 0.76$ . We simulate the time jitter noise as in the previous section. The results are shown in Fig. 6 where we plot the performance of the Bayesian estimator on noiseless and noisy test data for reference. We can see that the adversarially trained deep ensemble is much more robust to the shift in the input time delays than the single model and that the single model performs on par with the Bayesian inference method that does not model the noise in the input. This is useful for models that would be deployed to perform inference on data from measurement devices with different levels of noise than the ones used to generate the training data.

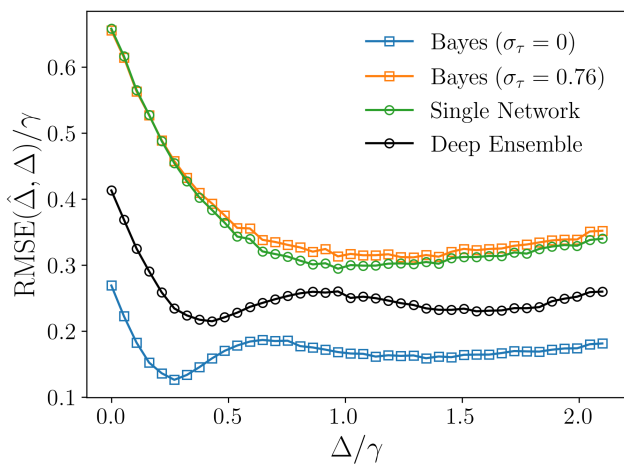
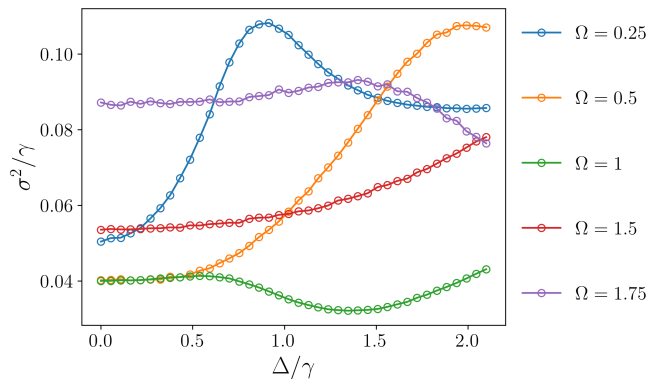
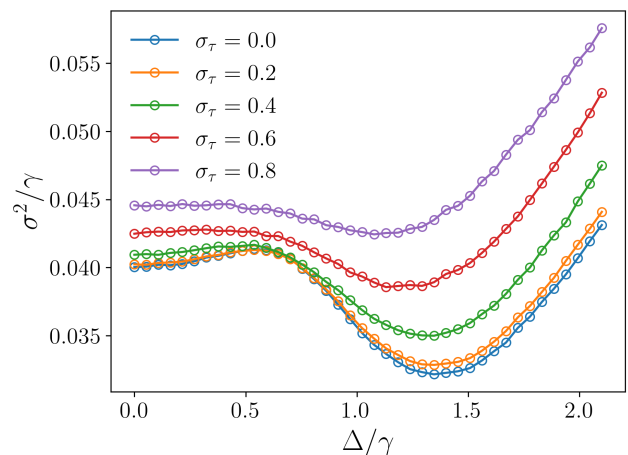


FIG. 6: Average RMSE of single network and adversarial deep ensemble trained on training data with no noise and evaluated on test data with time jitter noise with  $\sigma_\tau = 0.76$ . Bayesian inference on noiseless test data is plotted for reference.



(a) Average predicted variance  $\sigma^2$  from deep ensemble for test data (time delay measurements) generated from the training distribution where  $\Omega = 1$  and from different distributions where  $\Omega \neq 1$ .



(b) Average predicted variance  $\sigma^2$  of deep ensemble for test data generated from the training distribution, which includes no time jitter noise, and test data with time jitter noise following the Gaussian distribution  $\mathcal{N}(0, \sigma_\tau)$ .

FIG. 7: Predictive uncertainty of deep ensemble under different types of dataset shift.

## 2. Uncertainty quantification under data shift

An important property to examine for models which provide uncertainty estimates is how the predicted uncertainty changes when the model is provided out-of-distribution examples e.g. in the case of data shift [29]. Ideally we would want our model to have higher predictive uncertainty when given input data from a distribution that is far from the training distribution i.e. we would expect the predicted Gaussian mixture to have greater variance  $\sigma^2$ . Fig. 7a shows the average predicted uncertainty of the deep ensemble model when given sets of time delays from systems in which the Rabi frequency differs from the value used to generate the training data. We can see that as the Rabi frequency deviates further

from  $\Omega = 1$  the predictive uncertainty of our model increases.

This can be used to detect drift in the experimental data at inference time analogous to what has been demonstrated in Ref. [47] for image classification in industrial processes. For instance if one trains a deep ensemble on time delay data which were generated using a detector with minimal time jitter noise we would expect the ensemble, at inference time, to produce larger uncertainty estimates when presented with time delay measurements generated using a detector with time jitter noise. We can see that this is indeed the case in Fig. 7b which shows the average predicted uncertainty from an ensemble model, which was trained on time delay data with no jitter noise, for trajectories generated using varying levels of time jitter noise. This can be useful as a way of detecting imperfections or miscalibration in the experimental setup (in this case detector defectiveness) used to generate the time delay results given to the model at inference time.

### F. Posterior approximation

In addition to providing uncertainty estimates another benefit provided by our ensemble approach, which is similarly unavailable for currently existing single network approaches, is the ability to provide a smooth probability distribution over possible parameter values similar to the Bayesian inference approach. Naturally one may ask, given the uniform prior used in the Bayesian analysis and the universal approximation property of Gaussian mixtures, if we can expect the ensembles output distribution to have good fidelity with the Bayesian posterior. We provide an example of the Bayesian posterior and the ensemble mixture distribution for a single trajectory in Fig. 8 which suggests that this is indeed possible. To examine this further we compute the average fidelity between the Bayesian posterior distribution and the distribution learned by the ensemble over 100 random trajectories for each unique value of  $\Delta$  in our test set. As done in Ref. [13] we compute the fidelity between the analytic posterior and the mixture distribution learned by the ensemble as the Bhattacharyya coefficient

$$F(p_A(\theta), p_B(\theta)) = \int_{\Theta} \sqrt{p_A(\theta)p_B(\theta)} d\theta. \quad (9)$$

The results are shown in Fig. 9. We can see that for the majority of  $\Delta$  values the distribution learned by the ensemble has strong overlap with the Bayesian posterior. The fidelity degrades slightly near resonance values  $\Delta \approx 0$  as the uniform prior leads to an abrupt vanishing of the posterior density for values of  $\Delta < 0$  leading to a non-smoothly varying distribution near these values unlike the one always produced by the ensemble. Additionally, these values being close to the limit of the range of  $\Delta$  values,  $[0, 5\gamma]$ , used in the training data of the ensemble likely exacerbates the discrepancies.

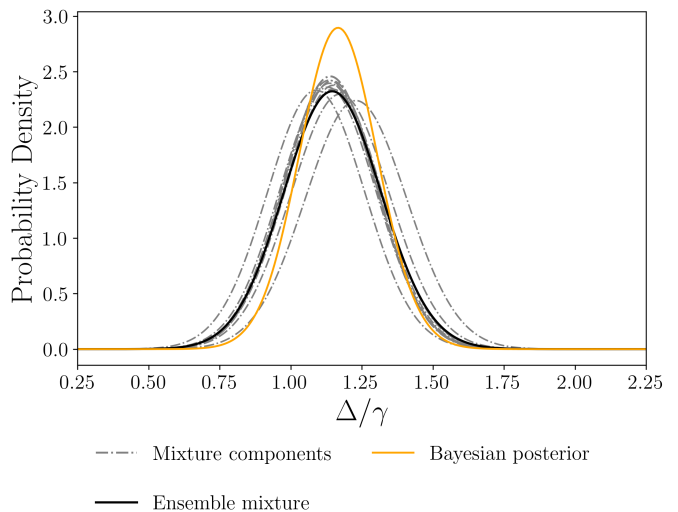


FIG. 8: Posterior distribution computed with a uniform prior over  $\Delta \in [0, 5\gamma]$  and mixture distribution learned by the ensemble for an example trajectory generated with  $\Delta \approx 1$  and  $\Omega = 1$ .

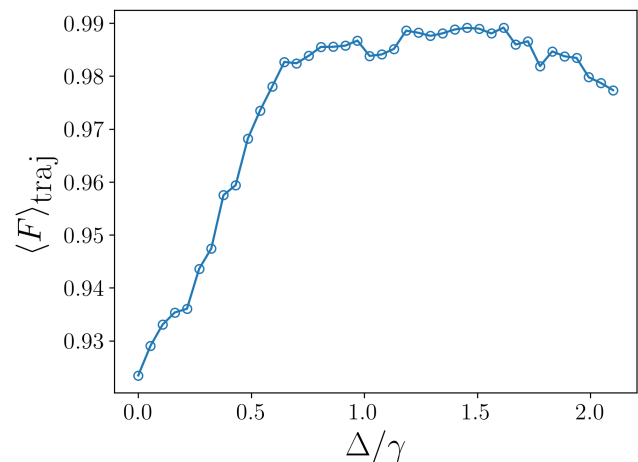


FIG. 9: Average fidelity between Bayesian posterior and ensemble Gaussian mixture distributions over 100 random trajectories per  $\Delta$  value.

### G. Multi-parameter estimation

Here we demonstrate our approach applied to the simultaneous estimation of the Rabi frequency  $\Omega$  and detuning  $\Delta$ . We train an ensemble of  $M = 10$  networks on  $16 \times 10^4$  trajectories of length  $N = 48$  which were generated using random values of  $\Delta \in [0, 3\gamma]$  and  $\Omega \in [0.25\gamma, 5\gamma]$  drawn uniformly from their respective intervals. We compare our ensembles performance to that of standard Bayesian inference performed using nested sampling [48, 49]. To avoid the prohibitively long inference time on our computational resources associated with

the two-dimensional Bayesian inference routine we evaluate the trained deep ensemble on the test set of trajectories from Ref. [21] whose precomputed Bayesian point estimates for the test set trajectories are made available at [35]. The test set contains  $16 \times 10^6$  trajectories to ensure convergence of the computed RMSEs and a uniform prior was used over the interval from which the training set was generated from to ensure fair comparison. Fig. 10 shows the RMSE achieved by both the deep ensemble and Bayesian inference. We can see that both approaches perform comparably with the deep ensemble often achieving a lower RMSE particularly for parameter values close to the boundaries of the parameter space under consideration. This shows that not only can the deep ensemble exceed the inference speed of likelihood-based Bayesian inference but that it can also achieve better performance in terms of estimation accuracy.

## H. Comparison to Approximate Bayesian Computation

Here we will compare the performance of our likelihood-free parameter inference method with the state-of-the-art likelihood-free method presented in Ref. [13] i.e. approximate Bayesian computation (ABC). For this comparison we consider the more complex optomechanical system studied in the same work.

### 1. Quantum system

The system consists of an optical cavity which is driven by an external laser with one of the mirrors being free to oscillate which constitutes the mechanical mode of the system [13, 50]. The Hamiltonian of the closed system is given by

$$\hat{H} = -\Delta \hat{a}^\dagger \hat{a} + \omega_M \hat{b}^\dagger \hat{b} + \frac{\Omega}{2} (\hat{a} + \hat{a}^\dagger) + g \hat{a}^\dagger \hat{a} (\hat{b} + \hat{b}^\dagger) \quad (10)$$

where  $\hat{a}$  and  $\hat{b}$  are the annihilation operators of the optical and mechanical modes respectively,  $\Omega$  is the laser Rabi frequency,  $g$  is the optomechanical coupling strength, and  $\omega_M$  is the mechanical frequency. The mechanical mode interacts with a thermal bath by both emitting and absorbing phonons while the optical mode leaks photons which are continuously detected. The master equation for the open system is given by

$$\frac{\partial}{\partial t} \hat{\rho}(t) = -i[\hat{H}, \hat{\rho}(t)] + \kappa \left( \hat{a} \hat{\rho}(t) \hat{a}^\dagger - \frac{1}{2} \{ \hat{a}^\dagger \hat{a}, \hat{\rho}(t) \} \right) \quad (11)$$

$$+ \gamma (\bar{m} + 1) \left( \hat{b} \hat{\rho}(t) \hat{b}^\dagger - \frac{1}{2} \{ \hat{b}^\dagger \hat{b}, \hat{\rho}(t) \} \right) \quad (12)$$

$$+ \gamma \bar{m} \left( \hat{b}^\dagger \hat{\rho}(t) \hat{b} - \frac{1}{2} \{ \hat{b} \hat{b}^\dagger, \hat{\rho}(t) \} \right) \quad (13)$$

where  $\bar{m} = (\exp(\omega_M/k_B T) - 1)^{-1}$  is the mean phonon number of the bath,  $T$  is the temperature of the bath,  $\kappa$  is the decay rate of the optical mode and  $\gamma$  is the decay rate of the mechanical mode.

Specifically, we consider the nonlinear regime of the system which arises when the coupling strength between the optical and mechanical modes is strong [13] and therefore the analytic Gaussian formalism is no longer sufficient to describe the system dynamics [50]. In this case no analytic solution to the master equation is available [13], which precludes the derivation of a likelihood function, thus necessitating the use of likelihood-free methods such as ABC. Notably one can set the detuning value as  $\Delta_n = -ng^2/\omega_M$ , where  $n \in \mathbb{Z}^+$ , so that  $n$ -photon emissions become favored by the system resulting in photon bunching in the  $n \geq 2$  regime [13, 50]. Note that the data used here has  $g = 4$  and  $\omega_M = 4\sqrt{2}$  [13].

### 2. Predictive accuracy benchmark

We train our deep ensemble to again minimize the Gaussian negative log likelihood loss. For the training data we use the data library from Ref. [13]. The data contains time delay trajectories of 80 photon detections for 100 evenly spaced values of the detuning  $\Delta$  across the range  $[-10, 0]$  with 4,000 trajectories for each unique  $\Delta$ . We randomly split the library using an 80/20 split between training and testing data and stratify by  $\Delta$  value to ensure each set is balanced and that we use a uniform prior for the ABC algorithm as done in [13]. Due to the nature of the dynamics of the system in the nonlinear regime, i.e. the system can generally not be approximated as a coherent state and assumed to reset to a consistent state with each photon detection like in the case of the TLS, the assumption of independence and identical distribution of the time delays in a given trajectory no longer holds. While these additional time delay correlations allow for potential improvement in the ability to perform sensing tasks [50] they also lead to the smoothed histogram neural network layer used previously no longer being optimal.

Two tools that are more appropriate in this setting are recurrent neural network layers such as a long-short term memory layer or a one-dimensional convolutional layer. We use the latter as it is generally simpler to implement and more amenable to parallelization than recurrent architectures [51]. The specific architecture of the deep ensemble networks are given in Appendix C. We use an ensemble of  $M = 10$  networks with  $\beta_1 = 0.87$ ,  $\beta_2 = 0.93$ , a learning rate of  $10^{-3}$  for the Adam optimizer, and a batch size of 250 over 50 epochs.

When benchmarking the ABC method we treat the training data as the data library. While the pseudocode for the ABC algorithm is given in Ref. [13] we give a more detailed implementation in Algorithm 1 for completeness. We draw  $\nu = 10^5$  samples and set  $\epsilon = 9$  as this was found to be more than enough for the method

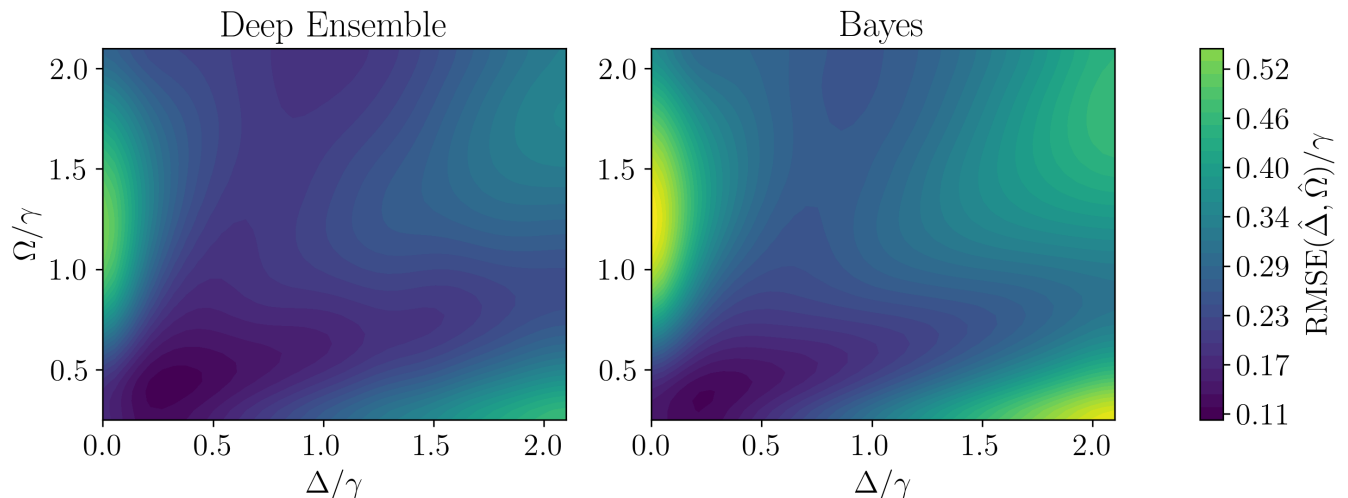


FIG. 10: Contour plots of average RMSE achieved by the deep ensemble and Bayesian inference via nested sampling on test set.

---

**Algorithm 1** Approximate Bayesian computation algorithm

---

**Require:** Library of trajectory-parameter pairs  $\mathcal{D}$ , number of times to sample from the library  $\nu$ , acceptance threshold for sample  $\epsilon$ , summary statistic function  $S(\cdot)$ , discrepancy measure function  $\delta(\cdot)$ , observed trajectory to perform parameter inference on  $D$

- 1: Initialize empty histogram  $H$  of  $\theta$ 's
- 2:  $i \leftarrow 0$
- 3: **while**  $i < \nu$  **do**
- 4: Sample, without replacement, one trajectory-parameter pair  $(D', \theta)$  from  $\mathcal{D}$
- 5: **if**  $\delta(S((D', \theta)), S(D)) \leq \epsilon$  **then**
- 6:  $H[\theta] \leftarrow H[\theta] + 1$   $\triangleright$  Add one count to histogram bin corresponding to value  $\theta$
- 7: **end if**
- 8:  $i \leftarrow i + 1$
- 9: **end while**
- 10: Normalize  $H$
- 11: **return**  $H$   $\triangleright$  Return the normalized histogram which serves as an approximation of the Bayesian posterior

---

to converge for estimation of the same parameter and data in [13]. We also use the same histogram based summary statistic and  $L_2$  discrepancy measure from [13] and similarly take the mean of the ABC posterior as our estimator of the parameter. Fig. 11 shows the performance of the two methods on our test set. We can see that for most values of  $\Delta$  the deep ensemble achieves lower error than ABC and achieves competitive accuracy in all other cases. Interestingly, for the  $\Delta_{n=3}$  regime we see that the ensemble greatly outperforms the ABC method suggesting it makes better use of the information encoded in the three-photon correlations present in the trajectory data. Note also that the inference time for the the ABC method is also about two orders of magnitude larger as we shall see in the next section.

#### IV. COMPUTATIONAL EFFICIENCY

Here we more closely examine the advantage provided by NNs in terms of their computational efficiency with respect to inference time and memory overhead particularly when compressed for deployment on edge devices such as FPGAs. The deep ensembles discussed thus far have a memory size of roughly 1.1 megabytes. This can be further compressed via the use of model quantization which converts the 32-bit floating point weights of the model to 8-bit integers. This reduces the size of our models to roughly 8.8 kilobytes. This contrasts with a method such as ABC which requires the storage of the data library during inference time and thus has a space complexity which is linear in the size of the dataset. This is valuable in cases where one wishes to deploy these models to edge devices with limited memory to perform real time inference and does not lead to any noticeable

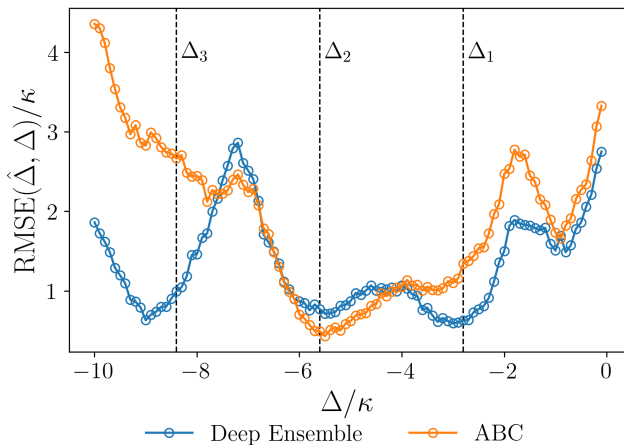
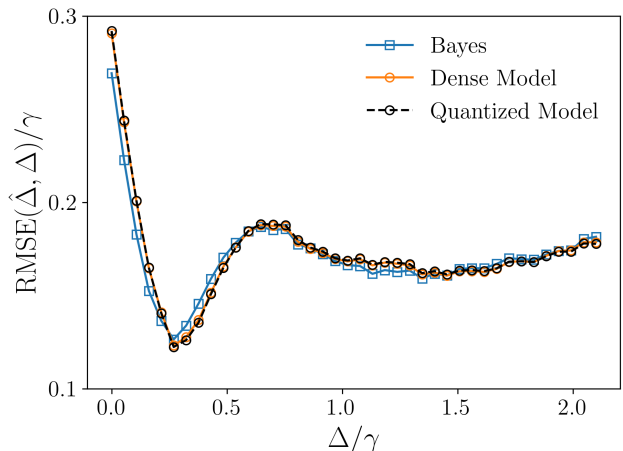


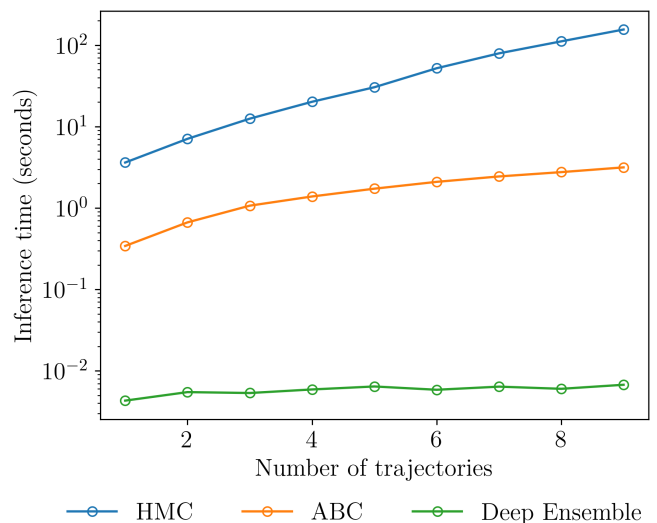
FIG. 11: Performance of ABC and deep ensemble on the test set for the nonlinear optomechanical system.

deterioration of model performance as can be seen in Fig. 12a. Other memory optimization methods, such as weight pruning, can be performed if further memory efficiency is required.

We also compare inference times by measuring the wall clock time of a trained quantized deep ensemble, the ABC method and an optimized likelihood-based Hamiltonian Monte Carlo (HMC) Bayesian inference routine for estimating  $\Delta$  given delay measurements from different numbers of trajectories. We use the state-of-the-art No U-Turn Sampler (NUTS) provided by the PyMC framework as our specific HMC method [52, 53]. For inference with NUTS we use 4 chains and draw 1,000 posterior samples per chain which we parallelize over 4 cores. For inference with ABC we use the same implementation of the algorithm used in the previous section which leverages NumPy array vectorization [54] when possible to ensure fair comparison. The average inference time for the three methods over 20 different runs of the inference on an AMD Ryzen 9 3900X 12-Core Processor are shown in Fig. 12b. We can see that the highly parallelizable nature of neural network inference, i.e. batched inference, allows for orders of magnitude faster inference speed over the NUTS and ABC method despite the need to perform a forward pass for each of the 10 NNs in the deep ensemble. The ability to parallelize inference with a neural network, due to the fact that the network is carrying out simple linear algebraic operations, contrasts with the inherently sequential nature of MCMC based Bayesian inference, due to the construction of the Markov chains, and ABC based Bayesian inference due to the rejection sampling routine. This shows that deep ensembles are better equipped for real time quantum parameter estimation tasks while still retaining the uncertainty quantification capabilities of Bayesian inference.



(a) Average RMSE of non-quantized deep ensemble and quantized deep ensemble.



(b) Average inference times over 10 runs for HMC based and ABC based Bayesian inference and quantized deep ensemble for various numbers of trajectories.

FIG. 12: Predictive accuracy and inference time of Bayesian inference and quantized deep ensemble.

## V. CONCLUSION

We have proposed a method for using NNs to perform parameter estimation which provides uncertainty estimates in addition to point estimates of the parameters. We showed that these models provide good parameter estimates despite being optimized for both predictive accuracy and uncertainty estimation. We also show that they provide well calibrated uncertainty estimates and good approximations of the Bayesian posterior distribution. We also demonstrated our scheme is applicable to more complex systems in which the measurement results are not independent and identically distributed, unlike

the case of the TLS studied in much of the present work, where recurrent or convolutional NNs become more appropriate to use over the permutation-invariant architectures discussed initially. Furthermore, our method can, in principle, be generalized to  $n$ -dimensional estimation problems by only adding an additional  $O(n)$  neurons in the output layer of the network as opposed to classification based approaches [20]. We have demonstrated this for the  $n = 2$  case in the present work. We leave higher dimensional extensions for future work along with the exploration of other NN architectures, such as deep sets, that possess permutation invariance and the ability to naturally handle inputs of varying length [55].

In this work we performed hyperparameter tuning on a single model and used the optimal hyperparameters from that search to train the deep ensemble due to time constraints. An interesting question to answer would be if hyperparameter tuning on the ensemble level, while being more computationally expensive, could deliver even better results. We also only considered ensembles in which all models have the same architecture but this is by no means a necessity. Further exploration of how using ensembles of networks with different architectures, e.g. different activation functions and numbers of hidden layers, would impact ensemble performance on the parameter estimation task would be useful, in particular with respect to how this affects the uncertainty estimates as this approach may better capture epistemic (model) uncertainty. Finally, since photon counting is not necessarily the most optimal measurement in terms of the quantum Fisher information (QFI) [21] it would be interesting to explore how the performance and data efficiency of these models changes when the QFI of the continuous measurement is optimized [56].

## ACKNOWLEDGMENTS

We thank Carlos Sánchez Muñoz, Tyree Giles, Derek Everett, Olivier Pfister and Aaron Reding for useful discussions.

## Appendix A: Bayesian Inference

The objective of Bayesian inference is to compute the posterior probability distribution  $P(\theta|D)$  where  $\theta$  is the parameter being estimated and  $D$  represents the observed data. From Bayes' rule the posterior is given by

$$P(\theta|D) = \frac{P(D|\theta)P(\theta)}{P(D)} \quad (\text{A1})$$

where  $P(D|\theta)$  is the likelihood,  $P(\theta)$  is the prior distribution over parameter values which can be chosen to incorporate our prior knowledge about the parameter, and  $P(D)$  is called the evidence or the marginal likelihood

[15, 16]. The Bayesian estimator,  $\hat{\theta}$ , of  $\theta$  is chosen to be either the mean, median or mode of the posterior with the posterior mean being the most common choice [57]. In our work we use the posterior mean  $\mathbb{E}[P(\theta|D)]$ . The delay time probability distribution for the TLS,  $w(\tau; \Delta, \Omega, \gamma)$ , which gives the probability density for a particular delay time  $\tau$  is given by [21]:

$$w(\tau; \Delta, \Omega, \gamma) = \frac{8\gamma\Omega^2}{R} e^{-\gamma\tau/2} \times \left( \sum_{\zeta=-1,1} \zeta \cosh \left( \frac{\tau \sqrt{\gamma^2 - 4(\Delta^2 + 4\Omega^2) + \zeta R}}{2\sqrt{2}} \right) \right) \quad (\text{A2})$$

where  $R = \sqrt{[\gamma^2 + 4(\Delta^2 + 4\Omega^2)]^2 - 64\gamma^2\Omega^2}$ . Using this the likelihood for a given set of time delay measurements  $D = [\tau_1, \dots, \tau_N]$  is given by

$$P(D|\theta) = \prod_{i=1}^N w(\tau_i; \Delta, \Omega, \gamma). \quad (\text{A3})$$

For our prior we use a uniform distribution with support on the range the training data was generated from for all experiments with the TLS.

The analytic expression of the posterior distribution is in general intractable to compute due to the denominator in Bayes' rule except for special cases such as conjugate prior-likelihood pairs. Due to this one must usually resort to simply drawing samples from the posterior distribution and computing summary statistics from these samples to perform inference. Markov chain Monte Carlo methods which draw (dependent) samples from our posterior distributions are the most common methods used in Bayesian inference as they completely circumvent the need to compute the denominator in Bayes rule [16]. An alternative approach which is more common in astrophysical studies is to use nested sampling [48, 49]. For the results presented in Section III we resort to numerically computing the posterior distribution by evaluating the denominator over a fine grid of 500 points on the support of the prior. Note that we do this as it is more exact for the case of a one-dimensional estimation problem but quickly becomes unwieldy for multi-dimensional problems.

## Appendix B: Hyperparameter Tuning Details

Hyperparameter tuning is an integral part of the ML training process particularly the *model selection* stage [34, 43]. If the number of hyperparameters is small and the possible values each can take on are as well then a simple grid search can be used to find the optimal set of hyperparameters. However this is impractical for most

modern deep learning models which can have many hyperparameters many of which are continuous in nature. Therefore much work has been done on hyperparameter tuning methods which are both fast and converge on a good set of hyperparameters. Methods based on Bayesian optimization such as the tree-structured Parzen estimator are the current state-of-the-art for hyperparameter tuning [38]. Table I shows the hyperparameters that were tuned during the model selection process as well as the search spaces for each hyperparameter.

Hyperparameter	Search Space
Number of histogram bins	(200, 710)
Loss function	{RMSE, MSLE}
Learning rate	$(10^{-5}, 5 \times 10^{-3})$
$\beta_1$ of Adam optimizer	(0.8, 0.999)
$\beta_2$ of Adam optimizer	(0.8, 0.999)
Number of epochs	(50, 500)
Batch size	$\{2^6, 2^7, 2^8, 2^9, 2^{10}, 2^{11}\}$
Dropout probability	(0, 0.2)
Early stopping patience	(4, 10)

TABLE I: Hyperparameters tuned during model selection with associated search spaces. Values in parenthesis indicate the lower and upper range of a search space whereas values in braces indicate the full discrete set of parameter values.

### Appendix C: Convolutional neural network architecture

Here we provide the specific architecture of the convolutional neural network used in Section III H in Table II.

- 
- [1] P. Kok and B. W. Lovett, Introduction to optical quantum information processing (Cambridge university press, 2010).
- [2] H. M. Wiseman and G. J. Milburn, Quantum measurement and control (Cambridge university press, 2009).
- [3] H. Yu, L. McCuller, M. Tse, N. Kijbunchoo, L. Barsotti, and N. Mavalvala, Quantum correlations between light and the kilogram-mass mirrors of ligo, *Nature* **583**, 43 (2020).
- [4] M. Tse, H. Yu, N. Kijbunchoo, A. Fernandez-Galiana, P. Dupej, L. Barsotti, C. Blair, D. Brown, S. e. Dwyer, A. Effler, et al., Quantum-enhanced advanced ligo detectors in the era of gravitational-wave astronomy, *Physical Review Letters* **123**, 231107 (2019).
- [5] J. Aasi, J. Abadie, B. Abbott, R. Abbott, T. Abbott, M. Abernathy, C. Adams, T. Adams, P. Addesso, R. Adhikari, et al., Enhanced sensitivity of the ligo gravitational wave detector by using squeezed states of light, *Nature Photonics* **7**, 613 (2013).
- [6] K. M. Backes, D. A. Palken, S. A. Kenany, B. M. Brubaker, S. Cahn, A. Droster, G. C. Hilton, S. Ghosh, H. Jackson, S. K. Lamoreaux, et al., A quantum enhanced search for dark matter axions, *Nature* **590**, 238 (2021).
- [7] A. J. Brady, C. Gao, R. Harnik, Z. Liu, Z. Zhang, and Q. Zhuang, Entangled sensor-networks for dark-matter searches, *PRX Quantum* **3**, 030333 (2022).
- [8] H. Shi and Q. Zhuang, Ultimate precision limit of noise sensing and dark matter search, *npj Quantum Information* **9**, 27 (2023).
- [9] A. H. Kiilerich and K. Mølmer, Estimation of atomic interaction parameters by photon counting, *Physical Review A* **89**, 052110 (2014).
- [10] S. Gammelmark and K. Mølmer, Bayesian parameter inference from continuously monitored quantum systems, *Physical Review A—Atomic, Molecular, and Optical Physics* **87**, 032115 (2013).
- [11] A. H. Kiilerich and K. Mølmer, Bayesian parameter estimation by continuous homodyne detection, *Physical Review A* **94**, 032103 (2016).
- [12] S. A. Sisson, Y. Fan, and M. Beaumont, Handbook of approximate Bayesian computation (CRC press, 2018).
- [13] L. A. Clark and J. Kołodyński, Efficient inference of quantum system parameters by approximate bayesian computation, *Physical Review Applied* **23**, 044040 (2025).
- [14] K. P. Murphy, Probabilistic machine learning: Advanced topics (MIT press, 2023).
- [15] A. Gelman, J. B. Carlin, H. S. Stern, and D. B. Rubin, Bayesian data analysis (Chapman and Hall/CRC, 1995).
- [16] B. Lambert, A student’s guide to Bayesian statistics (SAGE Publications Ltd, 2018).

TABLE II: Neural network architecture. The notation  $M \rightarrow N$  denotes a mapping from  $M$  features to  $N$  features.

Module	Configuration
<i>Convolutional Layers</i>	
Conv1d	1 $\rightarrow$ 100, kernel: 6, stride: 1, padding: 1
BatchNorm1d	100 features
ReLU	activation
Conv1d	100 $\rightarrow$ 200, kernel: 6, stride: 1, padding: 1
BatchNorm1d	200 features
ReLU	activation
<i>Dense Layers</i>	
Linear	200 $\rightarrow$ 128
BatchNorm1d	128 features
ReLU	activation
Linear	128 $\rightarrow$ 64
BatchNorm1d	64 features
ReLU	activation
Linear	64 $\rightarrow$ 32
BatchNorm1d	32 features
ReLU	activation
<i>Output Layer</i>	
Linear	32 $\rightarrow$ 2

- [17] J. Gawlikowski, C. R. N. Tassi, M. Ali, J. Lee, M. Humt, J. Feng, A. Kruspe, R. Triebel, P. Jung, R. Roscher, et al., A survey of uncertainty in deep neural networks, *Artificial Intelligence Review* **56**, 1513 (2023).
- [18] E. Greplova, C. K. Andersen, and K. Mølmer, Quantum parameter estimation with a neural network, arXiv preprint arXiv:1711.05238 (2017).
- [19] M. Khanahmadi and K. Mølmer, Time-dependent atomic magnetometry with a recurrent neural network, *Physical Review A* **103**, 032406 (2021).
- [20] S. Nolan, A. Smerzi, and L. Pezzè, A machine learning approach to bayesian parameter estimation, *npj Quantum Information* **7**, 169 (2021).
- [21] E. Rinaldi, M. G. Lastre, S. G. Herreros, S. Ahmed, M. Khanahmadi, F. Nori, and C. S. Munoz, Parameter estimation from quantum-jump data using neural networks, *Quantum Science and Technology* **9**, 035018 (2024).
- [22] É. Genois, J. A. Gross, A. Di Paolo, N. J. Stevenson, G. Koolstra, A. Hashim, I. Siddiqi, and A. Blais, Quantum-tailored machine-learning characterization of a superconducting qubit, *PRX Quantum* **2**, 040355 (2021).
- [23] V. Cimini, M. Valeri, E. Polino, S. Piacentini, F. Ceccarelli, G. Corrielli, N. Spagnolo, R. Osellame, and F. Sciarrino, Deep reinforcement learning for quantum multi-parameter estimation, *Advanced Photonics* **5**, 016005 (2023).
- [24] G. Cybenko, Approximation by superpositions of a sigmoidal function, *Mathematics of control, signals and systems* **2**, 303 (1989).
- [25] J. R. Johansson, P. D. Nation, and F. Nori, Qutip: An open-source python framework for the dynamics of open quantum systems, *Computer physics communications* **183**, 1760 (2012).
- [26] S. Narang, G. Damos, E. Elsen, P. Micikevicius, J. Alben, D. Garcia, B. Ginsburg, M. Houston, O. Kuchaiev, G. Venkatesh, et al., Mixed precision training, in *Int. Conf. on Learning Representation* (2017).
- [27] A. Paszke, S. Gross, F. Massa, A. Lerer, J. Bradbury, G. Chanan, T. Killeen, Z. Lin, N. Gimelshein, L. Antiga, et al., Pytorch: An imperative style, high-performance deep learning library, *Advances in neural information processing systems* **32** (2019).
- [28] T. Hastie, R. Tibshirani, J. H. Friedman, and J. H. Friedman, *The elements of statistical learning: data mining, inference, and prediction*, Vol. 2 (Springer, 2009).
- [29] B. Lakshminarayanan, A. Pritzel, and C. Blundell, Simple and scalable predictive uncertainty estimation using deep ensembles, *Advances in neural information processing systems* **30** (2017).
- [30] Y. Ovadia, E. Fertig, J. Ren, Z. Nado, D. Sculley, S. Nowozin, J. Dillon, B. Lakshminarayanan, and J. Snoek, Can you trust your model’s uncertainty? evaluating predictive uncertainty under dataset shift, *Advances in neural information processing systems* **32** (2019).
- [31] A. Thuy, *Learning Analytics with Neural Networks: Addressing Open*, Ph.D. thesis, Ghent University (2025).
- [32] A. Thuy and D. F. Benoit, Explainability through uncertainty: Trustworthy decision-making with neural networks, *European Journal of Operational Research* **317**, 330 (2024).
- [33] C. M. Bishop and H. Bishop, *Deep learning: Foundations and concepts* (Springer Nature, 2023).
- [34] I. Goodfellow, Y. Bengio, A. Courville, and Y. Bengio, *Deep learning*, Vol. 1 (MIT press Cambridge, 2016).
- [35] C. Sánchez Muñoz and E. Rinaldi, Dataset: Parameter estimation by learning quantum correlations in continuous photon-counting data using neural networks, 10.5281/zenodo.8305509 (2023).
- [36] L. A. Clark and J. Kolodynski, Efficient inference of quantum system parameters by approximate Bayesian computation - ABC libraries (2025).
- [37] S. Lee, S. Purushwalkam, M. Cogswell, D. Crandall, and D. Batra, Why m heads are better than one: Training a diverse ensemble of deep networks, arXiv preprint arXiv:1511.06314 (2015).
- [38] T. Akiba, S. Sano, T. Yanase, T. Ohta, and M. Koyama, Optuna: A next-generation hyperparameter optimization framework, in *Proceedings of the 25th ACM SIGKDD international conference on data mining* (2019) pp. 2623–2631.
- [39] M. Zaharia, A. Chen, A. Davidson, A. Ghodsi, S. A. Hong, A. Konwinski, S. Murching, T. Nykodym, P. Ogilvie, M. Parkhe, et al., Accelerating the machine learning lifecycle with mlflow., *IEEE Data Eng. Bull.* **41**, 39 (2018).
- [40] A. Anteneh, Dataset: Parameter estimation with uncertainty quantification from continuous measurement data using neural network ensembles, 10.5281/zenodo.17014659 (2025).

- [41] K. P. Murphy, Probabilistic machine learning: an introduction (MIT press, 2022).
- [42] J. C. López Carreño, E. Zubizarreta Casalengua, B. Silva, E. del Valle, and F. P. Laussy, Loss of antibunching, *Physical Review A* **105**, 023724 (2022).
- [43] G. James, D. Witten, T. Hastie, R. Tibshirani, and J. Taylor, An introduction to statistical learning: With applications in Python (Springer, 2023).
- [44] J. Quiñero-Candela, M. Sugiyama, A. Schwaighofer, and N. D. Lawrence, Dataset shift in machine learning (Mit Press, 2022).
- [45] S. Rabanser, S. Günnemann, and Z. Lipton, Failing loudly: An empirical study of methods for detecting dataset shift, *Advances in Neural Information Processing Systems* **32** (2019).
- [46] D. Hendrycks, K. Zhao, S. Basart, J. Steinhardt, and D. Song, Natural adversarial examples, in Proceedings of the IEEE/CVF conference on computer vision and pattern recognition (2021) pp. 15262–15271.
- [47] A. Thuy and D. F. Benoit, Fast and reliable uncertainty quantification with neural network ensembles for industrial image classification, *Annals of Operations Research* , 1 (2024).
- [48] J. Buchner, Nested sampling methods, *Statistic Surveys* **17**, 169 (2023).
- [49] F. Feroz and M. P. Hobson, Multimodal nested sampling: an efficient and robust alternative to markov chain monte carlo methods for astronomical data analyses, *Monthly Notices of the Royal Astronomical Society* **384**, 449 (2008).
- [50] L. A. Clark, B. Markowicz, and J. Kołodyński, Exploiting non-linear effects in optomechanical sensors continuous with photon-counting, *Quantum* **6**, 812 (2022).
- [51] A. Vaswani, N. Shazeer, N. Parmar, J. Uszkoreit, L. Jones, A. N. Gomez, L. Kaiser, and I. Polosukhin, Attention is all you need, *Advances in neural information processing systems* **30** (2017).
- [52] M. D. Hoffman, A. Gelman, et al., The no-u-turn sampler: adaptively setting path lengths in hamiltonian monte carlo., *J. Mach. Learn. Res.* **15**, 1593 (2014).
- [53] O. Abril-Pla, V. Andreani, C. Carroll, L. Dong, C. J. Fannesbeck, M. Kochurov, R. Kumar, J. Lao, C. C. Luhmann, O. A. Martin, et al., Pymc: a modern, and comprehensive probabilistic programming framework in python, *PeerJ Computer Science* **9**, e1516 (2023).
- [54] C. R. Harris, K. J. Millman, S. J. Van Der Walt, R. Gommers, P. Virtanen, D. Cournapeau, E. Wieser, J. Taylor, S. Berg, N. Jordán, et al., Array programming with numpy, *nature* **585**, 357 (2020).
- [55] M. Zaheer, S. Kottur, S. Ravanbakhsh, B. Póczos, R. R. Salakhutdinov, and A. J. Smola, Deep sets, *Advances in neural information processing systems* **30** (2017).
- [56] K. R. Chinni and N. Quesada, Optimal waveforms for dipole moment estimation with coherent states, *New Journal of Physics* (2026).
- [57] J. L. Devore, K. N. Berk, and M. A. Carlton, Modern mathematical statistics with applications (Springer Nature, 2021).